

Marker-based Visual SLAM leveraging Hierarchical Representations

Ali Tourani¹, Hriday Bavle¹, Jose Luis Sanchez-Lopez¹, Rafael Muñoz Salinas², and Holger Voos¹

Abstract—Fiducial markers can encode rich information about the environment and can aid Visual SLAM (VSLAM) approaches in reconstructing maps with practical semantic information. Current marker-based VSLAM approaches mainly utilize markers for improving feature detections in low-feature environments and/or for incorporating loop closure constraints, generating only low-level geometric maps of the environment prone to inaccuracies in complex environments. To bridge this gap, this paper presents a VSLAM approach utilizing a monocular camera along with fiducial markers to generate hierarchical representations of the environment while improving the camera pose estimate. The proposed approach detects semantic entities from the surroundings, including walls, corridors, and rooms encoded within markers, and appropriately adds topological constraints among them. Experimental results on a real-world dataset collected with a robot demonstrate that the proposed approach outperforms a traditional marker-based VSLAM baseline in terms of accuracy, given the addition of new constraints while creating enhanced map representations. Furthermore, it shows satisfactory results when comparing the reconstructed map quality to the one reconstructed using a LiDAR SLAM approach.

I. INTRODUCTION

Visual SLAM (VSLAM) systems can employ a wide range of vision sensors, such as monocular, stereo, Red Green Blue-Depth (RGB-D), omnidirectional, and event-based cameras to estimate the environmental map while localizing the camera [1]. The primary advantage of vision sensors is that they need low-cost hardware to supply rich visual and semantic information from surroundings for various tasks [2]. Semantic data, which refers to high-level information acquired from the environment, make VSLAM tasks more robust and expand the range of applications that can employ the reconstructed maps [1], [3]. For instance, robots may need to identify objects in the scene

¹Authors are with the Automation and Robotics Research Group, Interdisciplinary Centre for Security, Reliability, and Trust (SnT), University of Luxembourg, Luxembourg. Holger Voos is also associated with the Faculty of Science, Technology, and Medicine, University of Luxembourg, Luxembourg. {ali.tourani, hriday.bavle, jose.luis.sanchezlopez, holger.voos}@uni.lu

²Author is with the Department of Computer Science and Numerical Analysis, Rabanales Campus, University of Córdoba, Spain. rmsalinas@uco.es

This work was funded by the Institute of Advanced Studies (IAS) of the University of Luxembourg (project TRANSCEND), the European Commission Horizon2020 research and innovation program under the grant agreement No 101017258 (SESAME), and the Luxembourg National Research Fund (FNR) 5G-SKY project (ref. C19/IS/13713801).

For the purpose of Open Access, the author has applied a CC BY public copyright license to any Author Accepted Manuscript version arising from this submission.

The authors would like to thank Deniz İşınsu Avşar and Jan P.F. Lagerwall, both from the Department of Physics & Materials Science (DPHYMS) of the University of Luxembourg, for their efforts and valuable remarks on employing invisible fiducial markers as a futuristic scenario.

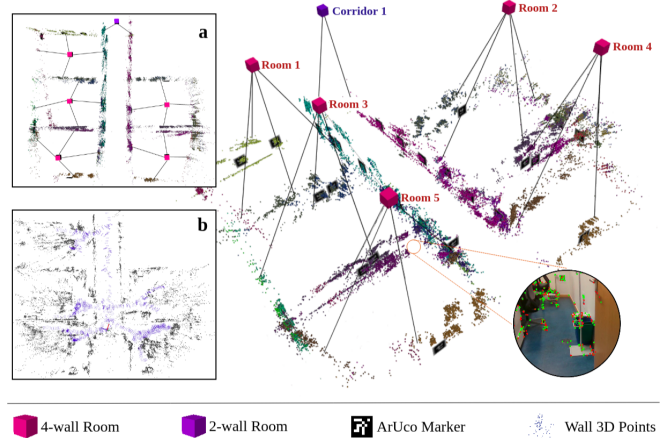


Fig. 1: The final reconstructed map of the environment using the proposed method in a hierarchical representation. Accordingly, the primary map entities are detected 3D points extracted from the environment and visited ArUco markers. Various colors of the 3D points refer to distinct walls, and the line connecting them to the cubes shows their belonging to rooms, including corridors or four-wall rooms: a) the top view of the reconstructed map represented in 2D, b) keypoints and robot trajectory records that lead to map reconstruction.

for path planning and dynamic object removal, which can be resolved using semantic data [4]. In this regard, utilizing fiducial markers is one of the possible approaches to encoding semantic information into the environment due to their rich and better-defined features [5]. In addition, they can assist VSLAM frameworks by providing accurate pose estimation due to their unique patterns, supplying reliable features in low-texture environments, and enabling loop closure detection based on marker identifiers. While most fiducial markers are visible to humans and, thus, visually polluting the environment, we have recently proposed novel *invisible fiducial markers* [6] that have the potential to be seamlessly integrated into the environment. Nevertheless, for the sake of simplicity, in this work, we use visible fiducial markers, leaving the use of *invisible fiducial markers* as future works. Recent works such as [7] and [8] propose VSLAM approaches using fiducial markers but do not encode them with meaningful semantic information, creating purely geometric map representations leading to inaccuracies in camera pose estimates and the generated environmental map in the presence of complex environments.

To fully leverage the potential of fiducial markers in accurately identifying both the semantic elements and their topo-

logical relationships while generating accurate and meaningful maps, this paper proposes a VSLAM framework for monocular cameras that utilizes the data encoded in fiducial markers for enhanced map reconstruction, adding abstract semantic elements to the final map along with their topological relationships. The system is built upon UcoSLAM [7], which employs ArUco [9] markers and visual keypoints extracted from natural landmarks reconstructing the geometric map of the environment using keypoints and markers. Additionally, inspired by *S-Graphs* [10], [11], leveraging high-level hierarchical representations for localization and mapping, the proposed approach adds extraordinary information in the form of walls, corridors, and rooms considering the data encoded in the ArUco markers attached to the environment. A sample map reconstructed by the proposed approach and its hierarchical representation is demonstrated in Fig. 1.

Herewith, the main contributions of the paper are summarized below:

- An extension of marker-based VSLAM to reconstruct environmental maps with high-level semantic features, including walls, corridors, and rooms, encoded within the markers,
- The design of novel geometric constraints, namely *marker-to-wall* and *wall-to-room*, to improve the map quality and reduce camera localization errors,
- Validation of the proposed method using a real-world indoor dataset showing improved performance over marker-based VSLAM baseline.

The rest of the paper is organized as follows: Section II explores previous efforts in the VSLAM domain, targeting the usage of semantic data for improved reconstructed maps. Section III introduces the proposed approach and its various modules in detail. In Section IV, the evaluation criteria and discussions over the effectiveness of the proposed method are provided. The paper finally concludes in Section V.

II. RELATED WORKS

VSLAM approaches have matured over the past years and many researchers contributed to this community by proposing efficient solutions to unresolved challenges in this area. The authors of this paper also presented a comprehensive survey on diverse VSLAM state-of-the-art works and studied their trade-offs in [12]. Accordingly, many recent approaches focus on improving the *front-end* thread of the VSLAM systems for better pose estimation and visual odometry [13]. Authors in [7] proposed UcoSLAM that employs both natural and artificial landmarks in the environment to reconstruct the map. It works in keypoints-only, markers-only, and mixed modes and improves the global map builder and loop closure detector modules in case ArUco markers are found in the camera’s field of view. Another marker-based approach titled TagSLAM [8] was proposed by Pfrommer and Daniilidis, which uses the capability of AprilTag [14] fiducial markers for SLAM tasks. Although the proposed approaches perform well in many scenarios, they cannot obtain any semantic information from the environment for an improved map

representation. Gomez-Ojeda *et al.* [15] introduced PL-SLAM, which uses Oriented FAST and Rotated BRIEF (ORB) and Line Segment Detector (LSD) algorithms to extract visual features of points and lines in stereo vision cameras. However, this approach is computationally intensive in feature tracking and extracting data from structural lines. Bruno and Colombini [16] proposed LIFT-SLAM, which integrates deep learning-based and conventional geometry-based feature descriptors. Despite the robust feature detection and tracking performance, the method uses an un-optimized Convolutional Neural Network (CNN), which leads to almost real-time execution.

Utilizing semantic data is another topic that attracted great attention in recent years. Gonzalez *et al.* [17] presented S³LAM, a monocular approach based on ORB-SLAM 2.0 [18] that uses semantic segmentation of generic objects and structures. Their approach fits a plane using the triangulated 3D points for each a priori planar cluster and uses a CNN-based panoptic segmentation framework titled *Detectron2* [19]. Likewise, YOLO-SLAM [20] is another CNN-based approach that couples geometric constraints with the Darknet19-YOLOv3 object detector to generate semantic information. However, these solutions may suffer from performance degradation in recognizing small or non-regular objects and planes. QuadricSLAM [21] is another approach that models objects found in the environment by employing quadric representations as object descriptions and estimates quadric parameters using object detection bounding boxes. This monocular VSLAM represents an object’s size, position, and orientation for map reconstruction. The main challenge of QuadricSLAM is the initialization stage, where a variety of viewing angles of the object is required. Hosseinzadeh *et al.* [22] proposed another monocular VSLAM system that inserts visited objects detected by a deep learning-based object detector and the dominant structure of the scene using a planar landmark detector to the map. Despite the robust performance, estimating the prior shape of the objects leads to high computational complexity. Another semantic VSLAM approach titled Blitz-SLAM [23] combines the original masks and depth information of the objects and eliminates noise blocks formed by dynamic objects. Authors in [24] proposed a parallel framework titled SOLO-SLAM, which uses semantic attributes of map points and geometric constraints to filter dynamic objects and reconstruct an improved map. The main challenge here is losing a great deal of information in low-dynamic scenarios. MISD-SLAM [25] is another semantic approach equipped with real-time instance segmentation based on a pre-trained CNN and dynamic feature removal. However, the algorithm removes objects that are static only in some frames.

In contrast with the mentioned works, the proposed approach creates a map of the environment by utilizing semantic data encoded within markers instead of employing any object detector. Accordingly, walls and room constraints are estimated based on mathematical modeling obtained from keypoints and markers data, which does not significantly affect the performance of the system. Additionally, the

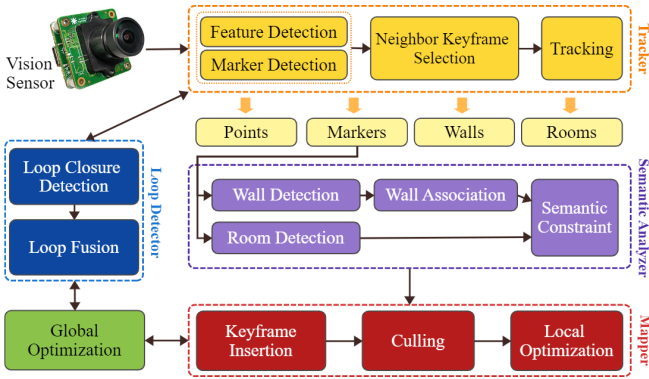


Fig. 2: The overall pipeline of the proposed approach. The main contributions of the proposed method are adding the *Semantic Analyzer* module and modifying the output of the *Tracker* to provide proper feed to it. Moreover, the *Global/Local Optimizer* modules have also been modified for better map reconstruction.

accuracy of the final reconstructed map of the environment is comparable with the one from Light Detection And Ranging (LiDAR)-based approaches, demonstrating the proposed method’s potential.

III. PROPOSED METHOD

The pipeline of the proposed method is depicted in Fig. 2. Accordingly, the frames captured by a monocular camera are passed to the system for processing. The *tracker* module detects ORB visual features and ArUco markers as the primary inputs of the system. Keyframes are selected and tracked over time, and the output contains 3D points, detected markers, walls, and rooms visited in the scene. The *semantic analyzer* module performs wall and room detection tasks using the pose of the markers detected in the *tracking* stage. Additionally, a *mapper* module handles adding new vertices and edges to the map and improves the final map for an optimized reconstruction. Finally, a marker-based *loop detector* module checks whether the markers in the current frame have been seen before and triggers the *global optimizer* to enhance the reconstructed map.

In order to develop a VSLAM framework with richer reconstructed maps, the proposed approach utilizes UcoSLAM as the baseline and modifies its components to be empowered with a semantic data analysis procedure. The mentioned modifications enable the detection of *walls* and different types of *rooms* as two semantic concepts in the environment using ArUco markers. Furthermore, as these fiducial markers are used for camera pose estimation, they can store additional encoded semantic data, which makes them an ideal alternative according to their unique identification properties. This method also aspires to employ visual data to represent the environment and the robot’s pose in a single optimizable graph with an approach comparable to *S-Graphs* [26]. Thus, instead of odometry readings and extracting planar surfaces using LiDAR scans introduced by *S-Graphs* and *S-Graphs+* [11], the proposed approach calculates the location of walls and

room variations using the fiducial markers attached to them.

A. Overview

The pipeline of the proposed method at time t can be referred to four main coordinate systems: the odometry frame of reference O , the camera coordinate system C_t , the marker coordinate system M_t , and the global coordinate system G_t . As the primary sensor of the system, a monocular camera acquires a set $\mathbf{F} = \{\mathbf{f}\}$ of frames $\mathbf{f} = \{t, \mathbf{T}, \delta\}$, where $\mathbf{T} \in SE(3)$ is the camera’s pose obtained from the transformation of C_t to G_t , and δ is the set of camera intrinsic parameters. By processing each camera frame using ORB keypoint detector and feature extractor, a set of keypoints $\mathbf{g} = \{l, u, \mathbf{d}\}$ are extracted in which l is the subsampling level of the image, u is the pixel coordinates for upsampling w.r.t. the first level, and $\mathbf{d} = (d_1 \dots d_n) | d_i \in [0, 1]$ is the descriptor vector with length n . Accordingly, the final constructed map of the environment \mathbf{E} will be represented as:

$$\mathbf{E} = \{\mathbf{K}, \mathbf{P}, \mathbf{M}, \mathbf{W}, \mathbf{R}\} \quad (1)$$

where $\mathbf{K} = \{k\} \subset \mathbf{F}$ is the set of keyframes and $\mathbf{P} = \{\mathbf{p}\}$ represents the set of feature points $\mathbf{p} = \{\mathbf{x}, \mathbf{v}, \hat{\mathbf{d}}\}$ extracted from the environment with their corresponding 3D positions $\mathbf{x} \in \mathbb{R}^3$, viewing direction $\mathbf{v} \in \mathbb{R}^3$, and descriptor $\hat{\mathbf{d}}$. Additionally, $\mathbf{M} = \{\mathbf{m}\}$ is the set of ArUco markers detected in the environment, in which each marker $\mathbf{m} = \{s, \mathbf{p}, \mathbf{cc}\}$ holds marker size (*i.e.*, length) $s \in \mathbb{R}$, marker pose $\mathbf{p} \in SE(3)$ calculated from M_t to G_t , and corner coordinates $\mathbf{cc} = (c_1 \dots c_4) | c_i \in \mathbb{R}^3$ values. The set of walls detected from the environment is represented by $\mathbf{W} = \{\mathbf{w}\}$, in which each wall $\mathbf{w} = \{\mathbf{q}, \mathbf{m}_w\}$ holds the wall equation $\mathbf{q} \in \mathbb{R}^4$ and the attached markers list $\mathbf{m}_w \subset \mathbf{M} = (m_1 \dots m_n) | m_i \in \mathbb{N}$ where m_i represents ArUco *marker-id*. Similarly, $\mathbf{R} = \{\mathbf{r}\}$ refers to the set of rooms found in the environment, where each room $\mathbf{r} = \{\mathbf{r}_c, \mathbf{r}_w\}$ contains the room center point $\mathbf{r}_c \in \mathbb{R}^3$ and the wall list $\mathbf{r}_w \subset \mathbf{W} = (w_1 \dots w_n) | w_i \in \mathbb{N}$ that comprise the room.

B. Semantic Entities

The proposed approach adds two semantic entities to construct a richer map, including *walls* and *rooms*. As detecting the mentioned entities is accomplished differently, the procedures are discussed in detail in this section.

Walls. The procedure to find the walls as plane-shaped entities on which the markers and their surrounding features are located is predominantly done using the pose information provided by detected ArUco markers. This approach assumes all fiducial markers are placed directly on the walls, not other elements such as radiators or drawer units. Thus, the equations of the walls are obtained based on the attached markers’ poses. The process of detecting walls in the scene occurs whenever a marker is being visited in a recent keyframe, making detecting and mapping the walls at a given time more efficient.

To add walls to the final map, each wall plane w_i is extracted in the global coordinate system ${}^G w_i = [{}^G \mathbf{n}_i \quad {}^G d]$

with a normal vector ${}^G\mathbf{n}_i = [n_x \ n_y \ n_z]^T$. The vertex node of the wall is factored in the graph as ${}^G\mathbf{w}_i = [{}^G\phi, {}^G\theta, {}^Gd]$, where ${}^M\phi$ and ${}^M\theta$ refer to the azimuth and elevation of the wall in G_t . For each marker ${}^G\mathbf{m}_i$ attached to the wall ${}^G\mathbf{w}_i$ cost function can be defined as:

$$c_{w_i}({}^G\mathbf{w}_i, {}^G\mathbf{m}_i) = \|[{}^M\delta\phi_{w_i m_i}, {}^M\delta\theta_{w_i m_i}, {}^M d_{w_i}]^T\|_{\Lambda_{\tilde{w}_i}}^2 \quad (2)$$

where ${}^M\delta\phi_{w_i m_i}$ difference between the azimuth angle of the wall w_i and its marker m_i converted to its marker frame M_i , ${}^M\delta\theta_{w_i m_i}$ is the difference in the elevation angles, while ${}^M d_{w_i}$ being the perpendicular distance between the wall and the marker, which should be zero the given marker-wall pair.

Rooms. Another semantic entity that has been considered in this work is the room. Since perceiving a room can be difficult due to various configurations and structures, the proposed approach employs the data encoded in ArUco markers attached to the room's walls to detect the mentioned semantic entity. In this regard, a dictionary containing the rooms in the environment and the fiducial markers attached to their walls are provided to feed the framework. Note that the only information encoded in the dictionary is the *marker-ids* corresponding to a room, and no additional pose information is required to be encoded. The proposed approach presents a modified version of the room segmentation process introduced in *S-Graphs+* [11], where the markers play a vital role. Hence, two room types titled "two-wall room" and "four-wall room" have been considered in this work:

Two-wall Rooms (Corridors): In this case, only two parallel walls of a room are labeled with fiducial markers. This scenario is proper for detecting corridors or rooms with undetectable/unreachable walls in the scene. Consequently, a room ${}^G\mathbf{r}_x = [{}^G\mathbf{w}_{x_{a_1}}, {}^G\mathbf{w}_{x_{b_1}}]$ contains x -wall planes parallel to the x -axis while ${}^G\mathbf{r}_y = [{}^G\mathbf{w}_{y_{a_1}}, {}^G\mathbf{w}_{y_{b_1}}]$ contains y -wall planes parallel to y -axis.

To compute the center of a two-wall room ${}^G\mathbf{r}_{x_i}$, the two x -wall plane equations are utilized along with the center point ${}^G\mathbf{c}_i$ of the marker \mathbf{m}_i as follows:

$${}^G\mathbf{k}_{x_i} = \frac{1}{2} [|{}^G d_{x_{a_1}}| \cdot {}^G\mathbf{n}_{x_{a_1}} - |{}^G d_{x_{b_1}}| \cdot {}^G\mathbf{n}_{x_{b_1}}] + |{}^G d_{x_{b_1}}| \cdot {}^G\mathbf{n}_{x_{b_1}} \\ {}^G\boldsymbol{\eta}_{x_i} = {}^G\hat{\mathbf{k}}_{x_i} + [{}^G\mathbf{c}_i - [{}^G\mathbf{c}_i \cdot {}^G\hat{\mathbf{k}}_{x_i}] \cdot {}^G\hat{\mathbf{k}}_{x_i}] \quad (3)$$

where ${}^G\boldsymbol{\eta}_{x_i}$ is the center point of the two-wall room ${}^G\mathbf{r}_{x_i}$ and ${}^G\hat{\mathbf{k}}_{x_i}$ is acquired from ${}^G\hat{\mathbf{k}}_{x_i} = {}^G\mathbf{k}_{x_i} / \|{}^G\mathbf{k}_{x_i}\|$. The center point ${}^G\mathbf{c}_i$ of the marker is obtained using the marker pose in frame G . It should be noted that a two-wall room center in the y direction can be calculated analogously.

A two-wall room node is initialized using the room center, and the cost function to minimize the two-wall room node and their corresponding wall planes are defined below:

$$c_{\mathbf{r}_{x_i}}({}^G\mathbf{r}_{x_i}, [{}^G\mathbf{w}_{x_{a_1}}, {}^G\mathbf{w}_{x_{b_1}}, {}^G\mathbf{c}_i]) \\ = \sum_{t=1, i=1}^{T, K} \|{}^G\hat{\boldsymbol{\eta}}_{x_i} - f({}^G\tilde{\mathbf{w}}_{x_{a_1}}, {}^G\tilde{\mathbf{w}}_{x_{b_1}}, {}^G\mathbf{c}_i)\|_{\Lambda_{\tilde{\mathbf{r}}_i, t}}^2 \quad (4)$$

where $f({}^G\tilde{\mathbf{w}}_{x_{a_1}}, {}^G\tilde{\mathbf{w}}_{x_{b_1}}, {}^G\mathbf{c}_i)$ maps the wall planes to the center point of the room using Eq. 3.

Four-wall Rooms: This scenario refers to rooms with four walls labeled with fiducial markers. In this regard, a four-wall room contains four wall planes as ${}^G\mathbf{r}_i = [{}^G\mathbf{w}_{x_{a_1}}, {}^G\mathbf{w}_{x_{b_1}}, {}^G\mathbf{w}_{y_{a_1}}, {}^G\mathbf{w}_{y_{b_1}}]$ forming the room. The center point of this variant of rooms can be computed using the equation below:

$${}^G\mathbf{q}_{x_i} = \frac{1}{2} [|{}^G d_{x_{a_1}}| \cdot {}^G\mathbf{n}_{x_{a_1}} - |{}^G d_{x_{b_1}}| \cdot {}^G\mathbf{n}_{x_{b_1}}] + |{}^G d_{x_{b_1}}| \cdot {}^G\mathbf{n}_{x_{b_1}} \\ {}^G\mathbf{q}_{y_i} = \frac{1}{2} [|{}^G d_{y_{a_1}}| \cdot {}^G\mathbf{n}_{y_{a_1}} - |{}^G d_{y_{b_1}}| \cdot {}^G\mathbf{n}_{y_{b_1}}] + |{}^G d_{y_{b_1}}| \cdot {}^G\mathbf{n}_{y_{b_1}} \\ {}^G\boldsymbol{\rho}_i = {}^G\mathbf{q}_{x_i} + {}^G\mathbf{q}_{y_i} \quad (5)$$

where ${}^G\boldsymbol{\rho}_i$ is the center point of the four-wall room ${}^G\mathbf{r}_i$. It should also be noted that Eq. 5 holds true when $|d_{x_1}| > |d_{x_2}|$. The cost function to minimize four-wall room nodes and their corresponding wall plane set is similar to a two-wall room but with minor differences:

$$c_{\boldsymbol{\rho}}({}^G\boldsymbol{\rho}, [{}^G\mathbf{w}_{x_{a_1}}, {}^G\mathbf{w}_{x_{b_1}}, {}^G\mathbf{w}_{y_{a_1}}, {}^G\mathbf{w}_{y_{b_1}}]) \\ = \sum_{t=1, i=1}^{T, S} \|{}^G\hat{\boldsymbol{\rho}}_i - f({}^G\tilde{\mathbf{w}}_{x_{a_1}}, {}^G\tilde{\mathbf{w}}_{x_{b_1}}, {}^G\tilde{\mathbf{w}}_{y_{a_1}}, {}^G\tilde{\mathbf{w}}_{y_{b_1}})\|_{\Lambda_{\tilde{\boldsymbol{\rho}}_i, t}}^2 \quad (6)$$

where $f({}^G\tilde{\mathbf{w}}_{x_{a_1}}, {}^G\tilde{\mathbf{w}}_{x_{b_1}}, {}^G\tilde{\mathbf{w}}_{y_{a_1}}, {}^G\tilde{\mathbf{w}}_{y_{b_1}})$ maps the four estimated wall planes to the center point of the four-wall room using Eq. 5. The above cost function maintains the structural consistency among the four walls forming the room.

C. Final Graph

Fig. 3 depicts the structure of the final semantic graph produced by the proposed approach. Accordingly, the keyframes extracted by the system are the primary sources of information that contain both visual feature points with their corresponding 3D coordinates and visited ArUco markers in the scene. It should be noted that the constraint defined among the keyframes, feature points, and fiducial markers is utilized for computing the odometry and for detecting loop closure. The wall-marker constraints are incorporated using Eq. 2. The topmost level of the graph retains rooms detected in the environment using the *marker-ids* and the walls that hold those markers with constraints obtained following Eq. 4 for two-wall rooms and Eq. 6 for four-wall rooms.

IV. EVALUATION

This section presents the proposed method's evaluation procedure in terms of accuracy and performance compared to the state-of-the-art approaches. In this respect, various real-world scenario tests were performed using the proposed

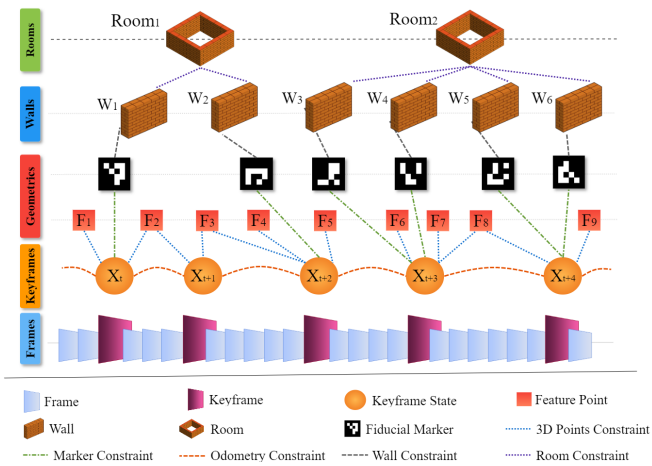


Fig. 3: The graph representation of the hierarchical architecture of the proposed approach. In this regard, the map employs new semantic constraints, including walls and rooms, along with geometrical constraints for better map reconstruction.



Fig. 4: Collected dataset for evaluation of the method: a) the legged robot used for data collection, b) some instances of the dataset.

method, UcoSLAM [7] as the baseline methodology, and *S-Graph+* [11] as a LiDAR-based approach for providing ground truth measurements. As LiDAR sensor has less noise when compared with the monocular vision-based sensor, it can be safely considered as ground truth.

A. Evaluation Setup

In order to evaluate the performance of the proposed approach in real-world circumstances, we mounted a *Intel® RealSense™ Depth Camera D435* as the monocular sensor on a *Boston Dynamics Spot®* robot and collected data from an indoor environment. The robot functioned in different office zones of two different university buildings with various corridor and room setups, where the walls were labeled with printed $17\text{cm} \times 17\text{cm}$ ArUco markers. *Marker-ids* of the ArUco markers placed in the environment, along with the room unique labels, were also stored in a database file and fed to the system. Fig. 4 demonstrates the robot employed for collecting data and some instances of the collected dataset. Additionally, the characteristics of the dataset are presented in Table I.

Evaluations have been conducted using a computer equipped with an *11th Gen. Intel® Core™ i9 @2.60GHz*

TABLE I: The characteristics of the collected indoors dataset.

Sequence*	Duration	#Markers	Description
Seq-01	08m 53s	35	Two corridors connected via a landing without robot rotation
Seq-02	09m 29s	35	Two corridors connected via a landing with robot rotation
Seq-03	16m 05s	26	One corridor and five rooms
Seq-04	10m 25s	14	One corridor and a two-doors room
Seq-05	09m 37s	20	Four aisles connected to a main corridor
Seq-06	23m 34s	22	Three corridors and three rooms

*data were stored as packages of *rosvbag* files.

processor and 32 GigaBytes of memory. Moreover, to better visualize the detected objects in the environment, including 3D points, ArUco markers, walls, and rooms, and provide a more accurate evaluation to compare the proposed method with other state-of-the-art approaches, a set of Robot Operating System (ROS) tools have been employed.

B. Experimental Results

In order to demonstrate the accuracy of the proposed method compared to its baseline and ground truth, Absolute Trajectory Error (ATE) measurements have been employed in this paper. Accordingly, the Root Mean Square Deviation (RMSE) and Standard Deviation (STD) values of the proposed and baseline approaches were compared to the ground truth, and the approach with less value is assumed to perform more accurately.

According to the evaluation results presented in Table II, the proposed approach works better than its baseline in most of the cases. The main reason for such improvement is the ability of the proposed method to add new constraints to the map and employ the association of semantic entities to enhance the reconstruction of the final map. The mentioned improvement can also be seen in Fig. 6. Moreover, the proposed approach utilizes data association results and performs a local *semantic loop closure* in addition to the marker-based loop closure detection when visiting a previously observed wall. In this regard, if the equation of the currently visible wall was previously measured, *i.e.*, the wall was previously detected, a global optimization runs again to improve the reconstructed map.

The above-mentioned impact is more obvious in cases such as *Seq-04* where the robot starts in a corridor, enters from one of the two doors of a room and exits from the other door to continue in the same corridor, and as a result, no loop closure using keypoints and markers is performed. While our method, which creates wall and room constraints, correctly identifies the corridor and its walls to provide better results. This improvement can be clearly seen in Fig. 5, where our method is able to reconstruct a more accurate map of the environment when compared with the baseline. Moreover, it is able to extract meaningful semantic and topological information from the environment.

Limitations. The proposed method, when testing in an environment where marker-based loop closure is triggered several times, can show similar results to baseline UcoSLAM.

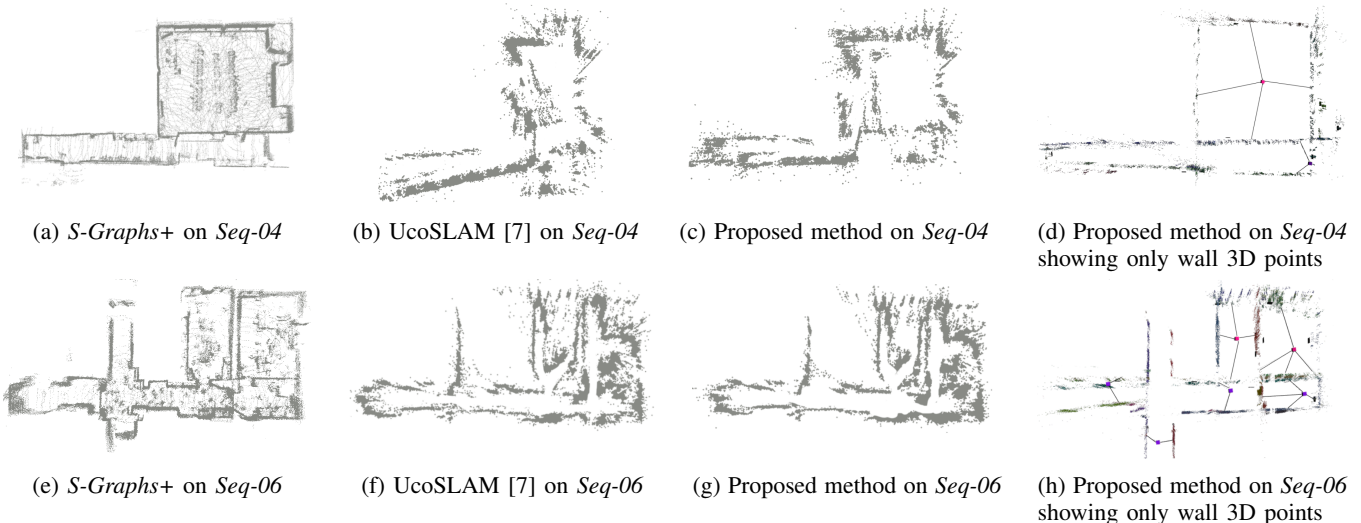


Fig. 5: Reconstructed maps using the proposed method, the baseline, and the ground truth. It can be seen that the proposed approach is able to generate more precise maps similar to the ground truth in detailed and with high-level semantic entities.

TABLE II: Evaluation results of the proposed method on the collected dataset using Root Mean Square Deviation (RMSE) error in *meters* and Standard Deviation (STD). The best results are boldfaced.

	Method			
	Proposed		UcoSLAM [7]	
Sequence	RMSE	STD	RMSE	STD
<i>Seq-01</i>	8.038	3.058	8.130	3.035
<i>Seq-02</i>	6.883	3.598	6.930	3.633
<i>Seq-03</i>	2.266	0.894	2.687	1.335
<i>Seq-04</i>	3.787	1.848	5.822	2.726
<i>Seq-05</i>	1.255	0.763	1.238	0.751
<i>Seq-06</i>	2.676	1.524	2.720	1.536

Seq-06 in Fig. 5 shows an example of the final map showcasing similar map quality results generated by the proposed method and UcoSLAM for an environment where the robot revisits the places (thus the markers) several times. Even with the given limitation for such scenarios, our approach is able to extract more meaningful information from the environment while maintaining similar accuracy with respect to the baseline.

V. CONCLUSIONS

This paper presented a Visual SLAM approach that employs a monocular camera as the sensor and the data encoded within fiducial markers placed in the surroundings for accurate pose estimation and semantic segmentation. The proposed method can detect three practical semantic entities in the environment, including walls, corridors, and rooms, and provide a hierarchical graph with high-level semantic data. Additionally, it can reconstruct a more accurate map of the environment by adding more topological constraints and employing the relations among mentioned semantic

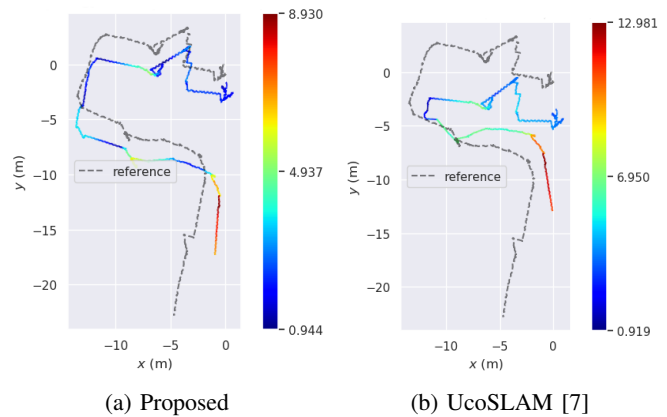


Fig. 6: Absolute Trajectory Error (ATE) w.r.t. translation part in *meters* on *Seq-04* using different approaches. It can be seen that the room created by the proposed approach is more similar to the ground truth.

entities found in the scene. Evaluations performed on a dataset collected by a legged robot in real-world conditions demonstrated an accuracy improvement compared to the baseline and satisfactory results compared to a LiDAR-based state-of-the-art techniques.

The approach proposed in this paper is part of a project which utilizes the advantages of fiducial markers for various tasks while keeping these markers invisible to human eyes but recognizable to robots. As for future works, the authors plan to encode the environment with the mentioned invisible fiducial markers introduced in [6] and equip the robot with a proper sensor setup to interpret them, making the improved version of the proposed approach able to accomplish Simultaneous Localization and Mapping tasks with the new type of markers. Additionally, improving the performance of the proposed system to work online and in real-time is another

target for future work.

REFERENCES

- [1] C. Cadena, L. Carlone, H. Carrillo, Y. Latif, D. Scaramuzza, J. Neira, I. Reid, and J. J. Leonard, "Past, present, and future of simultaneous localization and mapping: Toward the robust-perception age," *IEEE Transactions on robotics*, vol. 32, no. 6, pp. 1309–1332, 2016.
- [2] M. Filipenko and I. Afanasyev, "Comparison of various slam systems for mobile robot in an indoor environment," in *2018 International Conference on Intelligent Systems (IS)*. IEEE, 2018, pp. 400–407.
- [3] S. Han and Z. Xi, "Dynamic scene semantics slam based on semantic segmentation," *IEEE Access*, vol. 8, pp. 43 563–43 570, 2020.
- [4] S. Wen, P. Li, Y. Zhao, H. Zhang, F. Sun, and Z. Wang, "Semantic visual slam in dynamic environment," *Autonomous Robots*, vol. 45, no. 4, pp. 493–504, 2021.
- [5] J. Zhao, Y. Huang, X. He, S. Zhang, C. Ye, T. Feng, and L. Xiong, "Visual semantic landmark-based robust mapping and localization for autonomous indoor parking," *Sensors*, vol. 19, no. 1, p. 161, 2019.
- [6] H. Agha, Y. Geng, X. Ma, D. I. Avşar, R. Kizhakidathazhath, Y.-S. Zhang, A. Tourani, H. Bavle, J.-L. Sanchez-Lopez, H. Voos *et al.*, "Unclonable human-invisible machine vision markers leveraging the omnidirectional chiral bragg diffraction of cholesteric spherical reflectors," *Light: Science & Applications*, vol. 11, no. 1, pp. 1–19, 2022.
- [7] R. Muñoz-Salinas and R. Medina-Carnicer, "Ucoslam: Simultaneous localization and mapping by fusion of keypoints and squared planar markers," *Pattern Recognition*, vol. 101, p. 107193, 2020.
- [8] B. Pfrommer and K. Daniilidis, "Tagslam: Robust slam with fiducial markers," 2019. [Online]. Available: <https://arxiv.org/abs/1910.00679>
- [9] S. Garrido-Jurado, R. Muñoz-Salinas, F. J. Madrid-Cuevas, and M. J. Marín-Jiménez, "Automatic generation and detection of highly reliable fiducial markers under occlusion," *Pattern Recognition*, vol. 47, no. 6, pp. 2280–2292, 2014.
- [10] H. Bavle, J. L. Sanchez-Lopez, M. Shaheer, J. Civera, and H. Voos, "Situational graphs for robot navigation in structured indoor environments," 2022. [Online]. Available: <https://arxiv.org/abs/2202.12197>
- [11] —, "S-graphs+: Real-time localization and mapping leveraging hierarchical representations," *arXiv preprint arXiv:2212.11770*, 2022.
- [12] A. Tourani, H. Bavle, J. L. Sanchez-Lopez, and H. Voos, "Visual slam: What are the current trends and what to expect?" *Sensors*, vol. 22, no. 23, p. 9297, 2022.
- [13] I. A. Kazerouni, L. Fitzgerald, G. Dooly, and D. Toal, "A survey of state-of-the-art on visual slam," *Expert Systems with Applications*, p. 117734, 2022.
- [14] E. Olson, "Apriltag: A robust and flexible visual fiducial system," in *2011 IEEE international conference on robotics and automation*. IEEE, 2011, pp. 3400–3407.
- [15] R. Gomez-Ojeda, F.-A. Moreno, D. Zuniga-Noël, D. Scaramuzza, and J. Gonzalez-Jimenez, "PI-slam: A stereo slam system through the combination of points and line segments," *IEEE Transactions on Robotics*, vol. 35, no. 3, pp. 734–746, 2019.
- [16] H. M. S. Bruno and E. L. Colombini, "Lift-slam: A deep-learning feature-based monocular visual slam method," *Neurocomputing*, vol. 455, pp. 97–110, 2021.
- [17] M. Gonzalez, E. Marchand, A. Kacete, and J. Royan, "S3lam: Structured scene slam," *arXiv preprint arXiv:2109.07339*, 2021.
- [18] R. Mur-Artal and J. D. Tardós, "Orb-slam2: An open-source slam system for monocular, stereo, and rgb-d cameras," *IEEE transactions on robotics*, vol. 33, no. 5, pp. 1255–1262, 2017.
- [19] Y. Wu, A. Kirillov, F. Massa, W.-Y. Lo, and R. Girshick, "Detectron2," <https://github.com/facebookresearch/detectron2>, 2019.
- [20] W. Wu, L. Guo, H. Gao, Z. You, Y. Liu, and Z. Chen, "Yolo-slam: A semantic slam system towards dynamic environment with geometric constraint," *Neural Computing and Applications*, vol. 34, no. 8, pp. 6011–6026, 2022.
- [21] L. Nicholson, M. Milford, and N. Sünderhauf, "Quadricslam: Dual quadrics from object detections as landmarks in object-oriented slam," *IEEE Robotics and Automation Letters*, vol. 4, no. 1, pp. 1–8, 2018.
- [22] M. Hosseinzadeh, K. Li, Y. Latif, and I. Reid, "Real-time monocular object-model aware sparse slam," in *2019 International Conference on Robotics and Automation (ICRA)*. IEEE, 2019, pp. 7123–7129.
- [23] Y. Fan, Q. Zhang, Y. Tang, S. Liu, and H. Han, "Blitz-slam: A semantic slam in dynamic environments," *Pattern Recognition*, vol. 121, p. 108225, 2022.
- [24] L. Sun, J. Wei, S. Su, and P. Wu, "Solo-slam: A parallel semantic slam algorithm for dynamic scenes," *Sensors*, vol. 22, no. 18, p. 6977, 2022.
- [25] Y. You, P. Wei, J. Cai, W. Huang, R. Kang, and H. Liu, "Misdslam: multimodal semantic slam for dynamic environments," *Wireless Communications and Mobile Computing*, vol. 2022, 2022.
- [26] H. Bavle, J. L. Sanchez-Lopez, M. Shaheer, J. Civera, and H. Voos, "Situational graphs for robot navigation in structured indoor environments," *IEEE Robotics and Automation Letters*, vol. 7, no. 4, pp. 9107–9114, 2022.